

Luminescent hybrid materials of lanthanide β -diketonate and mesoporous host through covalent and ionic bonding with anion metathesis†

Qiu-Ping Li and Bing Yan*

Received 16th February 2012, Accepted 23rd May 2012

DOI: 10.1039/c2dt30364g

Luminescent mesoporous materials were prepared by performing an anion metathesis reaction on ionic liquid modified SBA15, which has imidazolium chloride bridging units. The lanthanide β -diketonate complex anion was successfully anchored onto the SBA15 framework after the anion metathesis reaction. The resulting materials were characterized by FTIR, TEM, TGA, small-angle X-ray powder diffraction (SAXRD) and nitrogen adsorption–desorption isotherms. The photoluminescent properties of these materials were investigated in detail, and the results reveal that these hybrid mesoporous SBA15, prepared through this preparation approach, present favorable photoluminescent behavior such as high luminescent quantum efficiencies and long luminescent lifetimes.

Introduction

The photophysical properties of lanthanide 1,3-diketonate (β -diketonate) complexes have attracted considerable attention in the past decades due to their potential applications in laser, optical amplifier and organic electroluminescent devices.¹ These complexes not only would preserve the merits of lanthanides in luminescence, such as high color purity and narrow band emission, but also can make use of the ligand to metal energy transfer mechanism (antenna effect²) to enhance the quantum efficiency of luminescence. Therefore, the synthesis of such luminescent lanthanide materials has been extensively studied in recent years. However, the practical applications of these compounds have been limited by their low thermal and photochemical stability, together with poor mechanical properties.³ Much work has been done to overcome these drawbacks by incorporating lanthanide β -diketonate complexes into inorganic matrices, such as silica-based sol–gel matrices. The resulting organic–inorganic materials are likely to combine the outstanding luminescent properties of the lanthanide β -diketonate complexes with the favorable thermal and mechanical characteristics of inorganic networks.⁴ Among these materials, lanthanide β -diketonate complexes functionalized ordered mesoporous silica is especially studied due to unique properties such as good hydrothermal and thermal stability, uniform pore structure and high surface area.⁵

Ionic liquids have attracted considerable attention within the past decades, owing to their potential application as environmentally benign solvents for chemical synthesis, separation, catalysis and electrochemistry.⁶ The prominent properties of an ionic

liquid such as negligible vapor pressure, thermal stability and widely tunable cation or anion have aroused wide public concern in material chemistry. The introduction of a metal ion complex anion can lead to a functional ionic liquid, which can combine the properties of ionic liquids with those properties such as catalytic, magnetic or photophysical properties that originate from the corresponding metal ion.⁷ Several approaches have been developed for preparing ionic liquid based hybrid materials including *in situ* or post polymerization of monomers, sol–gel processing in the ionic liquid, physical gelation, or impregnation into as-prepared matrices.⁸ Among these approaches, the method that anchors the ionic liquid to a specific supporting matrix followed by anion metathesis has been proven to be an effective way for constructing functional materials.⁹ Recently, a series of work has been done around highly luminescent lanthanide-containing ionic liquids, which show promising applications in constructing luminescent materials for use in photonics and photochemistry.¹⁰ Several kinds of materials have been synthesized by introducing lanthanide β -diketonate complexes into various matrices, which exhibit high quantum yields and good photochemical stability.¹¹

In this work, we put forward a novel method to construct luminescent mesoporous materials. In this case, the ionic liquid 1-methyl-3-[3-(trimethoxysilyl)propyl]imidazolium chloride is incorporated into the mesoporous SBA15 framework by an *in situ* sol–gel processing. Then, an anion metathesis processing is performed to introduce the lanthanide β -diketonate complexes anion. Four kinds of commercially available β -diketonates are used here; they are benzoyltrifluoroacetone (BTA), hexafluoroacetylacetone (HTA), thenoyltrifluoroacetone (TTA) and trifluoroacetylacetone (TAA). Subsequently, four europium based mesoporous materials SBA15- $\text{IM}^+[\text{Eu}(\text{L})_4]^-$ (L = TTA, BTA, HTA or TAA) are obtained after anchoring the europium β -diketonate complex anion onto the SBA15 framework. But for terbium based materials, because the triplet energy level

Department of Chemistry, Tongji University, Siping Road 1239, Shanghai, 200092, China. E-mail: byan@tongji.edu.cn; Fax: +86-21-65982287; Tel: +86-21-65984663

† Electronic supplementary information (ESI) available. See DOI: 10.1039/c2dt30364g

of TTA and BTA does not match the 5D_4 transition level of terbium, we have only selected HTA and TAA for constructing terbium based luminescent mesoporous materials. Moreover, all the resulting materials have been investigated in detail with respect to their characteristic and photoluminescent properties.

Experimental section

General

$\text{EuCl}_3 \cdot 6\text{H}_2\text{O}$ and $\text{TbCl}_3 \cdot 6\text{H}_2\text{O}$ are prepared according to a modified procedure reported in the literature¹² by dissolving their corresponding oxides (Eu_2O_3 , 99.9%, and Tb_2O_3 , 99.9%, Aladdin) in concentrated hydrochloric acid, followed by evaporation until the solutions become a pasty material. After that, the corresponding lanthanide chloride is collected by being filtered and washed with ice water and diethyl ether several times, subsequently. Tetraethoxysilane (TEOS, 99%, Aladdin) is distilled and stored under nitrogen atmosphere. Pluronic P123 ($\text{EO}_{20}\text{PO}_{70}\text{EO}_{20}$) is purchased from the Lancaster Company. (3-Chloropropyl)trimethoxysilane (CPTMO, 98%, Aladdin), 1-methylimidazole (99%, Aladdin), tetraethylammonium chloride (NEt_4Cl , 98%, Aladdin), trifluoroacetylacetone (TAA, 98%, Aladdin) and thenoyltrifluoroacetone (TTA, 98%, Aladdin), benzoyltrifluoroacetone (BTA, 99%, Aladdin) and hexafluoroacetylacetone (HTA, 98%, Aladdin) are used as received. All the other reagents are analytical pure and purchased from China National Medicines Group.

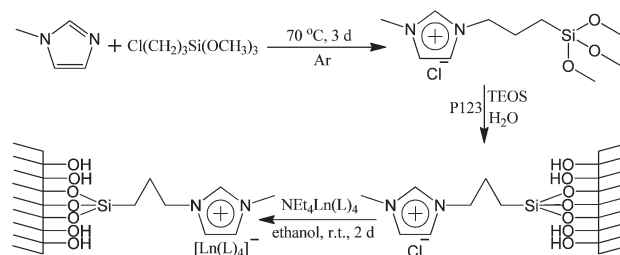
Synthesis procedure of 1-methyl-3-[3-(trimethoxysilyl)propyl]imidazolium chloride. The ionic liquid 1-methyl-3-[3-(trimethoxysilyl)propyl]imidazolium chloride is synthesized according to the procedure reported in the literature¹³ as follows: the 1-methylimidazole is mixed with one equiv. of CPTMO; the mixture is stirred at 70 °C for 3 d under argon atmosphere. Then, the pale-yellow viscous product is washed with anhydrous acetic ester three times. The resulting ionic liquid is dried overnight at 70 °C to remove the excess acetic ester under vacuum condition and denoted as IM^+Cl^- .

Synthesis of ionic liquid functionalized SBA15 ($\text{SBA15-IM}^+\text{Cl}^-$). The ionic liquid modified mesoporous material $\text{SBA15-IM}^+\text{Cl}^-$ is synthesized using a typical sol-gel processing¹⁴ with the molar ratio of P123 : TEOS : IM^+Cl^- : HCl : H_2O at 0.017 : 0.95 : 0.04 : 5.88 : 136. Typically, P123 (2 g) is dissolved in deionized water (7.5 g) at room temperature. Then a 2 M HCl solution (30 g) is added into the P123 solution. The mixture solution is then placed in a constant temperature (35 °C) oil bath. A mixture of TEOS and IM^+Cl^- is added to the above solution with stirring over 24 h and the mixture is transferred into a Teflon bottle sealed in an autoclave, which is heated to 100 °C for 2 d. The solid product is filtered off, washed with deionized water, and dried at 60 °C overnight. Removal of the template agent P123 is conducted by Soxhlet extraction with ethanol under reflux for 2 d. The resulting product is dried overnight at 50 °C under vacuum condition and denoted as $\text{SBA15-IM}^+\text{Cl}^-$.

Synthesis of lanthanide complexes $\text{NEt}_4\text{Ln}(\text{L})_4$ ($\text{Ln} = \text{Eu}, \text{Tb}$; $\text{L} = \text{TTA}, \text{BTA}, \text{HTA}$ or TAA). The lanthanide complexes are synthesized by using a modified literature procedure.¹⁵

For $\text{NEt}_4\text{Eu}(\text{TTA})_4$, typically: 0.888 g of TTA (4 equiv.) is dissolved in ethanol and deprotonated with 0.16 g NaOH (4 equiv.) at 60 °C for 2 h followed by the dropwise addition of 1 equiv. of $\text{EuCl}_3 \cdot 6\text{H}_2\text{O}$ in ethanol and by the addition of 1 equiv. of NEt_4Cl in ethanol. The mixture is kept at 60 °C for another 1 h. Then, the mixture is filtered to remove sodium chloride, and the filtrate is transferred to a flask for anion exchange. The synthesis procedures for $\text{NEt}_4\text{Eu}(\text{BTA})_4$, $\text{NEt}_4\text{Eu}(\text{HTA})_4$, $\text{NEt}_4\text{Eu}(\text{TAA})_4$, $\text{NEt}_4\text{Tb}(\text{HTA})_4$ and $\text{NEt}_4\text{Tb}(\text{TAA})_4$ are similar to that for $\text{NEt}_4\text{Eu}(\text{TTA})_4$.

Synthesis of lanthanide functionalized mesoporous materials $\text{SBA15-IM}^+[\text{Ln}(\text{L})_4]^-$ ($\text{Ln} = \text{Eu}, \text{Tb}$; $\text{L} = \text{TTA}, \text{BTA}, \text{HTA}$ or TAA). In order to perform anion exchange, the $\text{SBA15-IM}^+\text{Cl}^-$ is dispersed in the as-prepared $\text{NEt}_4\text{Ln}(\text{L})_4$ solution and stirred for 48 h at room temperature. The resulting material is collected by filtration and washed with ethanol. The excess $\text{NEt}_4\text{Ln}(\text{L})_4$ is removed by Soxhlet extraction with ethanol under reflux for 12 h. The resulting solid is dried overnight at 50 °C under vacuum condition and denoted as $\text{SBA15-IM}^+[\text{Eu}(\text{TTA})_4]^-$, $\text{SBA15-IM}^+[\text{Eu}(\text{BTA})_4]^-$, $\text{SBA15-IM}^+[\text{Eu}(\text{HTA})_4]^-$, $\text{SBA15-IM}^+[\text{Eu}(\text{TAA})_4]^-$, $\text{SBA15-IM}^+[\text{Tb}(\text{HTA})_4]^-$ and $\text{SBA15-IM}^+[\text{Tb}(\text{TAA})_4]^-$, respectively. The synthesis procedures and the possible structures of the resulting materials are shown in Scheme 1 and Fig. 1, respectively.



Scheme 1 Scheme of the synthesis procedures.

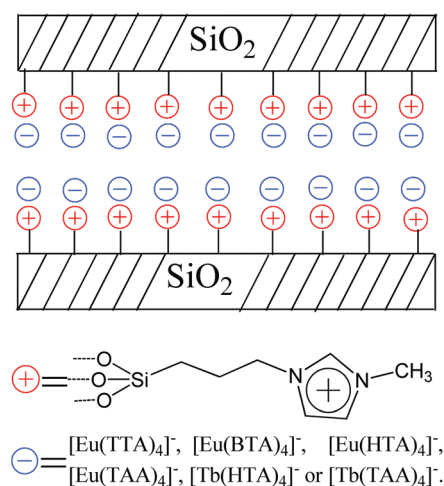


Fig. 1 Possible structure of the resulting materials.

Physical measurement

Fourier transform infrared spectra (FTIR) are measured within KBr slices from 4000–400 cm^{-1} using a Nexus 912 AO446 infrared spectrum radiometer. X-Ray powder diffraction patterns (XRD) are acquired on a Rigaku D/max-Rb diffractometer equipped with Cu anode; the data were collected within the 2θ range of 0.6–6°. Nitrogen adsorption and desorption isotherms are measured using a Nova 1000 system under the liquid nitrogen temperature. The Brunauer–Emmett–Teller (BET) method is used to calculate the surface of the mesoporous materials. Meanwhile, the Barrett–Joyner–Halenda (BJH) method is used to evaluate the pore size distribution and the other pore parameters. Thermogravimetric analysis (TG) is measured using a Netzsch STA 449C system at a heating rate of 5 $^{\circ}\text{C min}^{-1}$ under a nitrogen atmosphere. Transmission electron microscopy (TEM) experiments are performed using a JEOL2011 microscope operated at 200 kV. Luminescence excitation spectra, emission spectra and lifetimes (τ) are measured on an Edinburgh Instruments FLS 920 phosphorimeter. The diffuse reflectance UV-vis spectra of the powdered samples are recorded by a BWS003 spectrophotometer.

Results and discussion

The FTIR spectra of the precursor SBA15- IM^+Cl^- and selected lanthanide complex functionalized mesoporous materials are shown in Fig. 2. As shown in the FTIR spectra of SBA15- IM^+Cl^- , the characteristic absorbance for the bonds of an imidazole ring is found at 1570 cm^{-1} , suggesting that the ionic liquid IM^+Cl^- has been successfully immobilized onto the framework of mesoporous SBA15.¹⁶ Meanwhile the vibration of $-\text{CH}_2-$ appearing at about 2982 cm^{-1} further evidences the bonding of the ionic liquid. The broad bands appearing at 1080 cm^{-1} (ν_{as} , Si–O–Si), 795 cm^{-1} (ν_{s} , Si–O–Si) and 463 cm^{-1} (δ , Si–O–Si) indicate the success of hydrolysis and copolycondensation procedures, and the band located at 961 cm^{-1} is associated with the stretching vibrations of the silanol (Si–OH) of surface groups.¹⁷ Comparing the absorption spectrum of precursor SBA15- IM^+Cl^- with those of the lanthanide complex functionalized mesoporous materials, the new band at 1678 cm^{-1} (which is caused by the $-\text{C}=\text{O}$ group of β -diketone TTA, BTA, HTA or

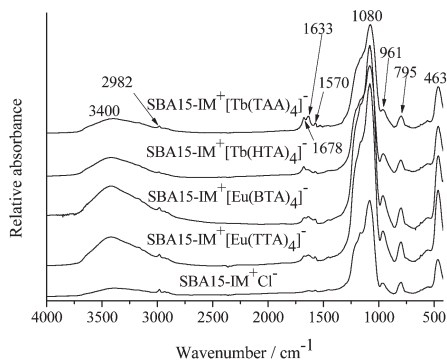


Fig. 2 The FTIR spectra for SBA15- IM^+Cl^- and different β -diketone based materials, and the lanthanide complex functionalized mesoporous materials.

TAA) indicates that the lanthanide complex anions have been successfully anchored onto the SBA15 frameworks by anion exchange. In addition, the broad band around 3400 cm^{-1} and the band at 1633 cm^{-1} can be ascribed as the bending and stretching vibrations of physically absorbed water,¹⁸ respectively.

One of the popular and efficient methods to characterize highly ordered mesoporous materials with hexagonal symmetry of the space group $P6mm$ is X-ray diffraction analysis. Fig. 3 shows the small-angle X-ray powder diffraction (SAXRD) patterns of precursor SBA15- IM^+Cl^- and the lanthanide complex functionalized mesoporous materials. It can be observed that all the patterns show three characteristic peaks of SBA15 in the 2θ range of 0.6–2°, including a prominent peak indexed as (100) at a low angle and two weaker peaks (110) and (200) at higher angles, suggesting that the ordered mesostructures have been well preserved in the final products. In addition, it is worth noticing that these functionalized mesoporous materials appear have decreased peak intensity, which is probably due to the decreasing of the degree of order after the introduction of the ionic liquid and the surface functionalization.

The other popular and efficient method to characterize highly ordered mesoporous materials is nitrogen adsorption–desorption isotherms, which could be used to explore the surface area, pore diameter and pore volume of the material. The N_2 adsorption–desorption isotherms of the precursor SBA15- IM^+Cl^- and the lanthanide complex functionalized mesoporous materials are presented in Fig. 4A and B. According to the IUPAC classification, SBA15 would show a type IV isotherm with a H1 type hysteresis loop at the high relative pressure region.¹⁹ In Fig. 4, it can be observed that all patterns show a slight deviation from the standard isotherm of pure SBA15, implying that the introduction of an ionic liquid and anion exchange with the lanthanide complexes slightly changes the pore regularities of the mesoporous material.²⁰ As shown in Fig. 4A, the N_2 adsorption–desorption isotherm for SBA15- IM^+Cl^- is just a little different to the other ones for the lanthanide complex functionalized mesoporous materials, indicating that the anion exchange processing hardly changes the morphology of the resulting materials. The specific area and the pore size have been calculated by using BET and BJH methods and listed in Table 1 together with the other structural parameters. It is worth noticing that these lanthanide complex functionalized mesoporous materials possessed a smaller BET surface area, pore volume and average pore

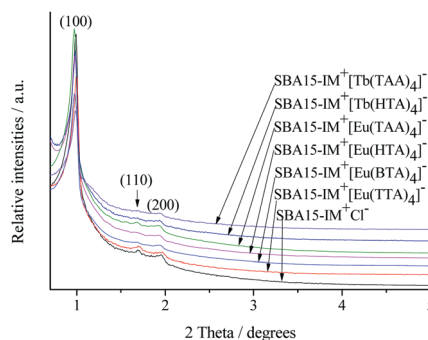


Fig. 3 XRD patterns for precursor SBA15- IM^+Cl^- and the resulted materials.

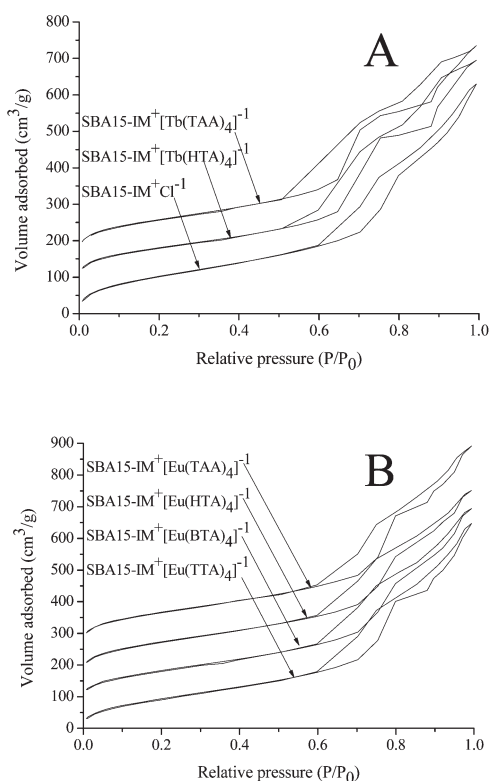


Fig. 4 N_2 adsorption-desorption isotherms for SBA15- IM^+Cl^- and final products.

Table 1 Structural parameters for SBA15- IM^+Cl^- and the resulted materials

Sample	d_{100} (nm)	a_0 (nm)	S ($m^2 g^{-1}$)	V ($cm^3 g^{-1}$)	D (nm)	t (nm)
SBA15- IM^+Cl^-	8.923	10.30	446.1	0.9895	7.501	2.803
SBA15- $IM^+[Eu(TTA)_4]^-$	8.909	10.29	424.4	0.9737	7.253	3.033
SBA15- $IM^+[Eu(TAA)_4]^-$	9.099	10.51	406.0	0.9094	6.578	3.929
SBA15- $IM^+[Eu(BTA)_4]^-$	9.098	10.50	447.9	0.8740	6.821	3.687
SBA15- $IM^+[Eu(HTA)_4]^-$	9.104	10.51	451.9	0.9077	7.053	3.459
SBA15- $IM^+[Tb(HTA)_4]^-$	9.010	10.40	407.8	0.9314	6.268	4.137
SBA15- $IM^+[Tb(TAA)_4]^-$	9.003	10.39	437.9	0.8918	6.952	3.444

d_{100} is the $d(1\ 0\ 0)$ spacing, a_0 the cell parameter ($a_0 = 2d_{100} \div \sqrt{3}$), S the BET surface area, V the total pore volume, D the average pore diameter, and t the wall thickness calculated by $a_0 - D$.

diameter than those typically reported for pure SBA15, suggesting that the incorporation of the ionic liquid and the subsequent anion exchange would reduce the pore volume of the samples, since the guests that are incorporated or coated inside the channels would enhance the roughness of the pore surface of the support. Additionally, the inflection positions have slightly shifted toward lower P/P_0 values, which also can be ascribed to the loading of guests into SBA15 frameworks.

The TEM images for SBA15- IM^+Cl^- and SBA15- $IM^+[Eu(TTA)_4]^-$ shown in Fig. 5A and B, respectively. It can be observed that the well-ordered hexagonal mesostructure is preserved in both SBA15- IM^+Cl^- and SBA15- $IM^+[Eu(TTA)_4]^-$, which is consistent with the results of the SAXRD patterns. As shown in the pictures, there is a regular hexagonal array of uniform two-dimensional channels, which also indicates that the mesostructure of SBA15 can be substantially conserved after the introduction of the ionic liquid and the subsequent anion exchange reaction. In addition, the distance between the contiguous centers of the mesopore is estimated to be about 10 nm, which is consistent with the results calculated from the corresponding SAXRD data (see Table 1). Furthermore, it can be also concluded through the comparison of the two TEM images that the anion exchange reaction has only a little effect on the morphology of the resulting materials.

To investigate the thermal stability of the obtained mesoporous materials, the thermogravimetric (TG) and the corresponding derivative weight loss (DTG) analysis were performed. Fig. 6 presents the TG and DTG curves of the SBA15- $IM^+[Eu(TTA)_4]^-$ at a heating rate of $5\ ^\circ C\ min^{-1}$ under nitrogen atmosphere. It is clear from the TG curve that three main degradation steps are observed. Combining with the DTG analysis, the first step of mass loss (about 15.0%) from 30 to 160 $^\circ C$ could be divided into two sections, for which, the initial faster weight loss of 4.5% observed up to 60 $^\circ C$ is due to the residual ethanol loaded during the anion metathesis process, and the latter weight loss of 10.5% is mainly attributed to the physically absorbed water. With further heating, the second step of weight loss

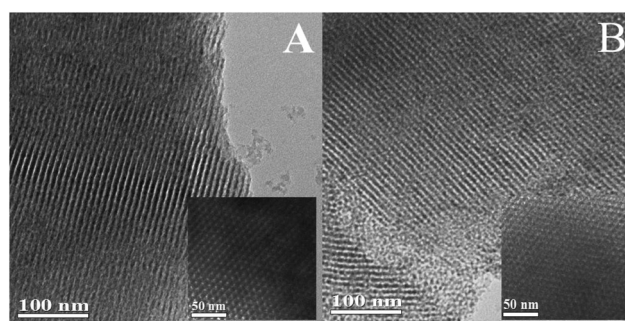


Fig. 5 TEM images of SBA15- IM^+Cl^- and SBA15- $IM^+[Eu(TTA)_4]^-$.

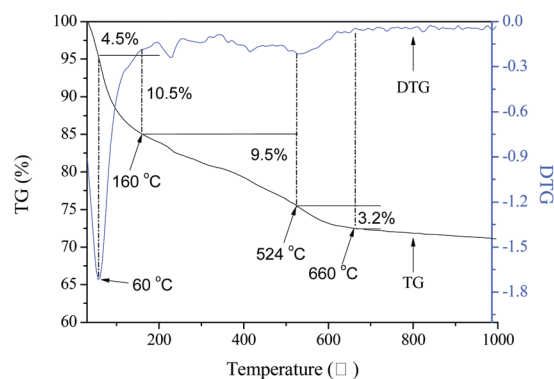


Fig. 6 TG and DTG curves for SBA15- $IM^+[Eu(TTA)_4]^-$.

(about 9.5%) from 160 to 524 °C can be observed, which may also be associated with two different weight loss reasons according to the DTG analysis. The weight loss from 160 to 227 °C can probably be attributed to europium tris chelates that have not been washed away, usually with the common formula $\text{Eu}(\text{TAA})_3 \cdot n\text{H}_2\text{O}$.²¹ The weight loss between 227 and 524 °C is associated with the decomposition of the organic moieties, which mainly refers to those europium tetrakis(β -diketonate) attaching onto the mesoporous frameworks through electrostatic interactions. Finally, the last weight loss of 3.2% beyond 524 °C is attributed to the decomposition of those organic parts that derived from the IM^+Cl^- , whose composition could be corresponded to a formula of $\text{C}_7\text{H}_{12}\text{N}_2\text{Cl}$. Comparing to the general decomposition temperature range of pure lanthanide complexes, our materials possess a wider decomposition temperature interval ranging from 227 to 524 °C, indicating that the thermal stability of the europium complex moieties was enhanced as they were introduced into the mesoporous silicon–oxygen matrix.^{21,22} Such enhanced thermal stability of lanthanide complexes when introducing them into an appropriate matrix has also been observed in the literature.²³ In addition, the residual weight of 75.5% when the sample is heated above 524 °C could be seen as a combined contribution of ionic liquid functionalized mesoporous material and the residual europium oxide. The europium oxide would occupy one third of the weight composition of the europium complex. Therefore, the reasonable percentage for residual europium oxide could take about half the weight loss value of 9.5%. That is to say, the weight percentage of the ionic liquid functionalized mesoporous material could be estimated to a value of 71%. Basing on the above discussion, the possible loading quantity of 4.5% of ionic liquid is deduced.

The diffuse reflectance UV-vis spectra measurements are performed for all powdered materials. Fig. 7A–C show the spectra of the precursor $\text{SBA15-IM}^+\text{Cl}^-$ and all the lanthanide complex functionalized mesoporous materials. It is clear from the figure that most of the resulting materials show an intense broad band adsorption among the ultraviolet region (250–400 nm), except for the HTA modified materials, which is attributed to the absorption of the β -diketone ligands (TTA, BTA or TAA). These adsorption bands also partially overlap with their own photoluminescence excitation spectra shown in Fig. 8. It can be primarily inferred that the energy levels between the β -diketone TTA (or BTA, TAA) and the europium ion match well, so that the organic ligand can sensitize the emission of the europium ion by energy transfer after it absorbs the ultraviolet light, and so can TAA for the terbium ion. Then, most of the final products can be expected to have excellent photoluminescence properties under the irradiation of ultraviolet light, which is proved in the luminescence spectra in Fig. 8. Unfortunately, it seems that the ligand HTA exhibits a weak adsorption in the ultraviolet region, although we can observe the luminescent spectra of HTA modified materials. In addition, a peak at 612 nm (Fig. 7A and B) also can be observed in the spectra, which is due to the corresponding europium ion.

The photoluminescence properties of the obtained lanthanide complex functionalized mesoporous materials have been investigated at room temperature and are shown in Fig. 8A–C. The excitation spectra of the europium complex functionalized materials are obtained by monitoring the characteristic emission

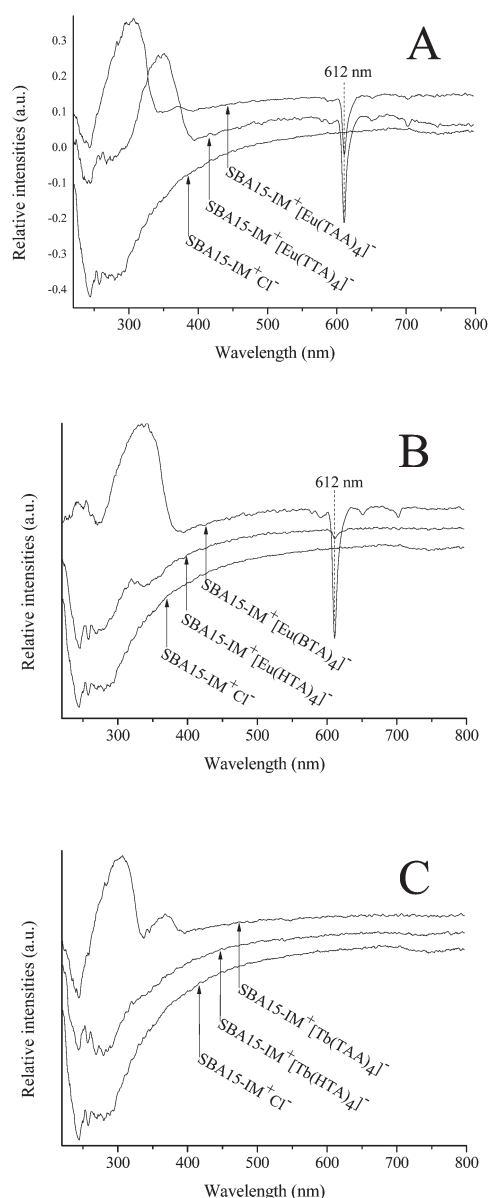


Fig. 7 The diffuse reflectance UV-vis spectra for $\text{SBA15-IM}^+\text{Cl}^-$ and the resulting lanthanide complex functionalized materials.

of the europium ion at 612 nm and presented in Fig. 8A and B. It is clear from the picture that both the materials have a broad band absorption in the range of 240–400 nm, suggesting the effective absorption of the materials. But, the maximum peaks for $\text{SBA15-IM}^+[\text{Eu}(\text{TAA})_4]^-$, $\text{SBA15-IM}^+[\text{Eu}(\text{BTA})_4]^-$, $\text{SBA15-IM}^+[\text{Eu}(\text{HTA})_4]^-$ and $\text{SBA15-IM}^+[\text{Eu}(\text{TAA})_4]^-$ centers at about 352, 357, 283 and 342 nm, respectively, which is attributed to the difference between the energy levels of different ligands. As a result, all the europium complex functionalized materials possess similar emission spectra that come from the characteristic europium ion emission. As shown in Fig. 7A and B, the emission lines located at around 578, 590, 612, 654 and 701 nm are assigned to ${}^5\text{D}_0 \rightarrow {}^7\text{F}_J$ (where $J = 0, 1, 2, 3, 4$). The spectra are dominated by a very intense ${}^5\text{D}_0 \rightarrow {}^7\text{F}_2$ transition at 612 nm, which is typical for europium β -diketonate complexes. It is well

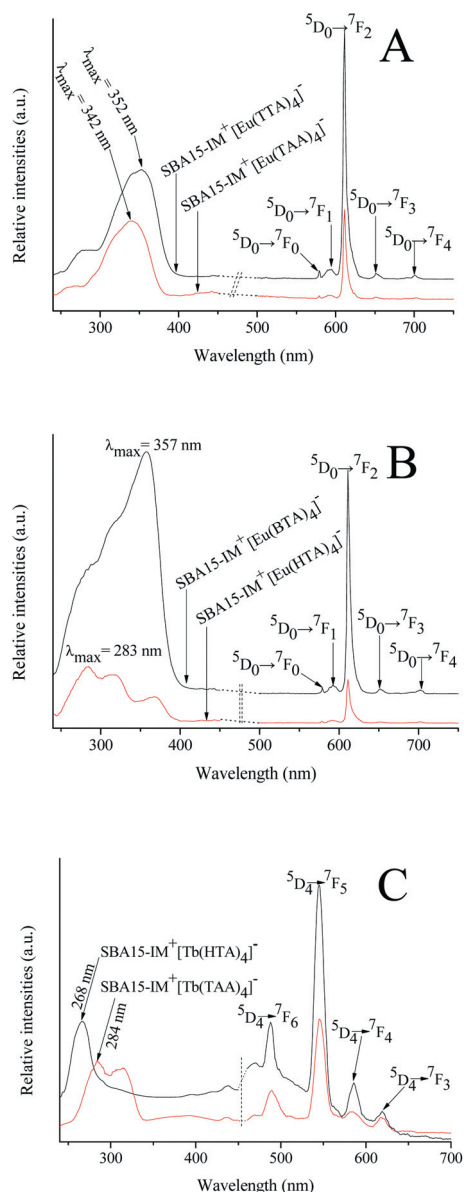


Fig. 8 Excitation and emission spectra for the lanthanide complex functionalized materials.

known that the $^5D_0 \rightarrow ^7F_2$ transition for the europium ion is a typical electric dipole transition, which is very sensitive to even small changes in their local environment,²⁴ while the parity-allowed magnetic dipole transition $^5D_0 \rightarrow ^7F_1$ is independent of the local environment of the europium ion.²⁵ As a result, the intensity ratios $I(^5D_0 \rightarrow ^7F_2)/I(^5D_0 \rightarrow ^7F_1)$ have been widely used as an indicator of the local environment of the europium ion. Based on the data, the intensity ratios $^5D_0 \rightarrow ^7F_2$ to $^5D_0 \rightarrow ^7F_1$ of all the europium complex functionalized materials are calculated and listed in Table 2, indicating the non-existence of an inversion center around the europium ion. In addition, we can find that the luminescent intensities of SBA15-IM⁺[Eu(TAA)₄]⁻ and SBA15-IM⁺[Eu(HTA)₄]⁻ are weaker than those of SBA15-IM⁺[Eu(TTA)₄]⁻ and SBA15-IM⁺[Eu(BTA)₄]⁻, indicating that the TTA and BTA ligands are the favorable sensitizers for the europium ion,²⁶ probably

Table 2 Luminescence data for the lanthanide complex functionalized mesoporous materials

Samples	I_{02}/I_{01} ^a	τ ^b (ms)	$1/\tau$ (s ⁻¹)	A_r	A_{nr}	η ^c (%)
SBA15- IM ⁺ [Eu(TTA) ₄] ⁻	14.68	685.2	1459	815.6	643.4	55.9
SBA15- IM ⁺ [Eu(BTA) ₄] ⁻	15.83	729.2	1371	853.9	517.1	62.3
SBA15- IM ⁺ [Eu(HTA) ₄] ⁻	9.82	82.8	12 077	576.6	11 500	4.8
SBA15- IM ⁺ [Eu(TAA) ₄] ⁻	14.32	317.5	3149	800.1	2349	25.4
SBA15- IM ⁺ [Tb(HTA) ₄] ⁻		18.5				
SBA15- IM ⁺ [Tb(TAA) ₄] ⁻		44.8				

^a The emission intensity ratios of the $^5D_0 \rightarrow ^7F_1$ transition (I_{01}) and the $^5D_0 \rightarrow ^7F_2$ transition (I_{02}). ^b Lifetimes (τ) of 5D_0 energy levels of the Eu³⁺ excited state. ^c (η value) is the luminescence quantum efficiency value from the measurement (*i.e.* outer luminescence quantum efficiency with error $\pm 10\%$).

because they possess a more asymmetrical molecular structure than TAA and HTA, in accordance with the above discussion.²⁷

In the same way, the excitation spectra of the terbium complex functionalized materials are shown in Fig. 8C, by monitoring the characteristic emission of the terbium ion at 545 nm. Both the SBA15-IM⁺[Tb(TAA)₄]⁻ and SBA15-IM⁺[Tb(HTA)₄]⁻ also possess a broad excitation spectrum, which is centered at 284 and 268 nm, respectively, it also can be associated with the ligand-to-metal charge transfer transition. The corresponding emission spectra of the terbium ion are presented and while no obvious f-f transitions are observed, four peaks between 450 and 650 nm can be clearly seen from it. These peaks transition at 487, 545, 582 and 621 nm, and are assigned to $^5D_4 \rightarrow ^7F_J$ (where $J = 6, 5, 4, 3$, respectively). Among these peaks, the peak located at 545 nm ($^5D_4 \rightarrow ^7F_5$), which gives the green luminescence, is the most intense one. Besides, we have found that the luminescence intensity of SBA15-IM⁺[Tb(HTA)₄]⁻ is slighter weaker than that for SBA15-IM⁺[Tb(TAA)₄]⁻, which is probably due to the HTA exhibiting a weaker adsorption in the ultraviolet region than TAA, according to the diffuse reflectance UV-vis spectra presented in Fig. 7C. Besides, we have found that the luminescence intensities of SBA15-IM⁺[Tb(TAA)₄]⁻ and SBA15-IM⁺[Tb(HTA)₄]⁻ are much weaker than those for SBA15-IM⁺[Eu(TAA)₄]⁻ and SBA15-IM⁺[Eu(HTA)₄]⁻ from the spectra data, indicating that the TAA and HTA are not very suited as sensitizers for the terbium ion, which can be ascribed to the mismatch of the triplet energy level of the ligands and the corresponding transition level of the terbium ion. In fact, a β -diketone group ligand is not the best one for sensitizing the luminescence of a terbium ion, by comparison with a carboxyl group ligand, because the 5D_4 transition level of the terbium ion is higher than the triplet level of most β -diketone group ligands.²⁸

In order to further explore the luminescence properties of these obtained materials, the typical decay curves of the lanthanide complex functionalized mesoporous materials were measured by using their own maximum excitation wavelength at room temperature. It can be expressed as an exponential

formation $[\ln(S_t/S_0) = -k_1t = -t/\tau]$, indicating that all the lanthanide ions occupy the same average coordination environment. The resulting luminescence lifetime values are listed in Table 2. As shown in the Table 2, the luminescence lifetimes of SBA15- $\text{IM}^+[\text{Eu}(\text{TAA})_4]^-$ and SBA15- $\text{IM}^+[\text{Eu}(\text{BTA})_4]^-$ are higher than the ones for SBA15- $\text{IM}^+[\text{Eu}(\text{TAA})_4]^-$ and SBA15- $\text{IM}^+[\text{Eu}(\text{HTA})_4]^-$, which is consistent with the results we concluded from their emission spectra. In addition, the luminescence lifetime of SBA15- $\text{IM}^+[\text{Tb}(\text{HTA})_4]^-$ is slightly lower than SBA15- $\text{IM}^+[\text{Tb}(\text{TAA})_4]^-$, which can be also attributed to its low adsorption in the ultraviolet region.

For the europium based materials, the emission quantum efficiency (η) of the emitting $^5\text{D}_0$ level can be determined on the basis of the emission spectra together with the lifetimes and can be calculated using the following equation²⁹ (detailed calculation process is given in ESI[†]).

$$\eta = \frac{A_r}{A_r + A_{nr}}$$

The quantum efficiencies of the europium based materials are shown in Table 2. It can be clearly seen that the luminescence quantum efficiencies of SBA15- $\text{IM}^+[\text{Eu}(\text{TAA})_4]^-$ (55.9%) and SBA15- $\text{IM}^+[\text{Eu}(\text{BTA})_4]^-$ (62.3%) are higher than those we previously reported for europium based mesoporous materials,³⁰ suggesting that this method is a preferable way for constructing europium based luminescent mesoporous materials. Meanwhile, the relatively high quantum efficiency of these materials shows that the SBA15 is an excellent host for the europium complexes.

Conclusions

In general, we have successfully designed and synthesized a series of luminescent mesoporous materials by incorporating an ionic liquid into the SBA15 framework in the synthesis procedure followed by anion exchange, which provides a novel method for assembling luminescent materials. All mesoporous materials are characterized and discussed in detail. The results demonstrate that all the resulting materials only show a slight change in their structure and morphology. Further investigation of the luminescence properties of these materials reveals that the lanthanide complex ions can be effectively anchored to the SBA15 framework through an imidazolium molecular bridge, and preserve their excellent characteristic emission that originated from the corresponding lanthanide ion. Efforts to research these kinds of materials modified by ionic liquid are currently under way in our group.

Acknowledgements

This work is supported by the National Natural Science Foundation of China (20971100, 91122003) and Program for New Century Excellent Talents in University (NCET-08-0398).

Notes and references

1 (a) L. N. Sun, H. J. Zhang, Q. G. Meng, F. Y. Liu, L. S. Fu, C. Y. Peng, J. B. Yu, G. L. Zheng and S. B. Wang, *J. Phys. Chem. B*, 2005, **109**,

- 6174; (b) L. N. Sun, H. J. Zhang, L. S. Fu, F. Y. Liu, Q. G. Meng, C. Y. Peng and J. B. Yu, *Adv. Funct. Mater.*, 2005, **15**, 1041; (c) K. Okada, M. Uekawa, Y. F. Wang, T. M. Chen and T. Nakaya, *Chem. Lett.*, 1998, 801; (d) J. Kido, K. Nagai and Y. Okamoto, *J. Alloys Compd.*, 1993, **192**, 30; (e) M. R. Robinson, M. B. O'Regan and G. C. Bazan, *Chem. Commun.*, 2000, 1645; (f) L. D. Carlos, R. A. S. Ferreira, V. D. Bermudez and S. J. L. Ribeiro, *Adv. Mater.*, 2009, **21**, 509; (g) K. Binnemans, *Chem. Rev.*, 2009, **109**, 4283.
- 2 (a) J. C. G. Bunzli and C. Piguet, *Chem. Soc. Rev.*, 2005, **34**, 1048; (b) N. Sabbatini, M. Guardigli and J. M. Lehn, *Coord. Chem. Rev.*, 1993, **123**, 201; (c) J. M. Lehn, *Rep. Prog. Phys.*, 2004, **67**, 249; (d) B. Alpha, R. Ballardini, V. Balzani, J.-M. Lehn, S. Perathoner and N. Sabbatini, *Photochem. Photobiol.*, 1990, **52**, 299; (e) P. Lenaerts, K. Driesen, R. Van Deun and K. Binnemans, *Chem. Mater.*, 2005, **17**, 2148.
- 3 H. R. Li, L. S. Fu, F. Y. Liu, S. B. Wang and H. J. Zhang, *New J. Chem.*, 2002, **26**, 674.
- 4 (a) H. R. Li, N. N. Lin, Y. G. Wang, Y. Feng, Q. Y. Gan, H. J. Zhang, Q. L. Dong and Y. H. Chen, *Eur. J. Inorg. Chem.*, 2009, 519; (b) J. Feng, J. B. Yu, S. Y. Song, L. N. Sun, W. Q. Fan, X. M. Guo, S. Dang and H. J. Zhang, *Dalton Trans.*, 2009, 2406; (c) X. M. Guo, H. D. Guo, L. S. Fu, H. J. Zhang, L. D. Carlos, R. P. Deng and J. B. Yu, *J. Photochem. Photobiol., A*, 2008, **200**, 318; (d) C. Sanchez, F. Ribot and B. Lebeau, *J. Mater. Chem.*, 1999, **9**, 35.
- 5 (a) Y. J. Li and B. Yan, *Inorg. Chem.*, 2009, **48**, 8276; (b) Y. J. Li and B. Yan, *Dalton Trans.*, 2010, **39**, 2554; (c) Y. J. Li and B. Yan, *J. Mater. Chem.*, 2011, **21**, 8129.
- 6 (a) J. P. Hallett and T. Welton, *Chem. Rev.*, 2011, **111**, 3508; (b) A. E. Visser and R. D. Rogers, *J. Solid State Chem.*, 2003, **171**, 109; (c) N. V. Plechkova and K. R. Seddon, *Chem. Soc. Rev.*, 2008, **37**, 123.
- 7 (a) B. Mallick, B. Balke, C. Felser and A. V. Mudring, *Angew. Chem., Int. Ed.*, 2008, **47**, 7635; (b) T. Nakashima, Y. Nonoguchi and T. Kawai, *Polym. Adv. Technol.*, 2008, **19**, 1401; (c) M. Li, P. J. Pham, C. U. Pittman and T. Y. Li, *Microporous Mesoporous Mater.*, 2009, **117**, 436.
- 8 (a) Y. H. Liu, X. Q. Sun, F. Luo and J. Chen, *Anal. Chim. Acta*, 2007, **604**, 107; (b) M. A. Neouze, J. Le Bideau, F. Leroux and A. Vioux, *Chem. Commun.*, 2005, 1082; (c) M. A. Neouze, J. Le Bideau, P. Gaveau, S. Bellayer and A. Vioux, *Chem. Mater.*, 2006, **18**, 3931; (d) N. Kimizuka and T. Nakashima, *Langmuir*, 2001, **17**, 6759.
- 9 (a) K. Lunstrook, K. Driesen, P. Nockemann, C. Gorller-Walrand, K. Binnemans, S. Bellayer, J. Le Bideau and A. Vioux, *Chem. Mater.*, 2006, **18**, 5711; (b) L. Maggini, H. Traboulsi, K. Yoosaf, J. Mohanraj, J. Wouters, O. Pietraszkiewicz, M. Pietraszkiewicz, N. Armadori and D. Bonifazi, *Chem. Commun.*, 2011, **47**, 1625; (c) M. Litschauer, M. Puchberger, H. Peterlik and M. A. Neouze, *J. Mater. Chem.*, 2010, **20**, 1269; (d) M. A. Neouze, *J. Mater. Chem.*, 2010, **20**, 9593.
- 10 (a) K. Binnemans, *Chem. Rev.*, 2005, **105**, 4148; (b) S. n. z, A. Babai, K. Binnemans, K. Driesen, R. Giernoth, A. V. Mudring and P. Nockemann, *Chem. Phys. Lett.*, 2005, **402**, 75; (c) H. R. Li, H. F. Shao, Y. G. Wang, D. S. Qin, B. Y. Liu, W. J. Zhang and W. D. Yan, *Chem. Commun.*, 2008, 5209; (d) A. Getsis, S. F. Tang and A. V. Mudring, *Eur. J. Inorg. Chem.*, 2010, 2172.
- 11 (a) S. F. Tang and A. V. Mudring, *Eur. J. Inorg. Chem.*, 2009, 2769; (b) K. Lunstrook, K. Driesen, P. Nockemann, L. Viau, P. H. Mutin, A. Vioux and K. Binnemans, *Phys. Chem. Chem. Phys.*, 2010, **12**, 1879; (c) K. Lunstrook, K. Driesen, P. Nockemann, K. Van Hecke, L. Van Meervelt, C. Gorller-Walrand, K. Binnemans, S. Bellayer, L. Viau, J. Le Bideau and A. Vioux, *Dalton Trans.*, 2009, 298; (d) P. Nockemann, E. Beurer, K. Driesen, R. Van Deun, K. Van Hecke, L. Van Meervelt and K. Binnemans, *Chem. Commun.*, 2005, 4354; (e) S. M. Bruno, R. A. S. Ferreira, F. A. A. Paz, L. D. Carlos, M. Pillinger, P. Ribeiro-Claro and I. S. Goncalves, *Inorg. Chem.*, 2009, **48**, 4882.
- 12 M. S. Tarasenko, N. G. Naumov, A. V. Virovets, D. Yu. Naumov, N. V. Kuratieva, Yu. V. Mironov, V. N. Ikorskii and V. E. Fedorov, *J. Struct. Chem.*, 2005, **46**, S137.
- 13 (a) C. P. Mehnert, *Chem.-Asian J.*, 2004, **11**, 50; (b) C. M. Zhong, T. Sasaki, M. Tada and Y. Iisawa, *J. Catal.*, 2006, **242**, 357.
- 14 D. Y. Zhao, Q. S. Huo, J. L. Feng, B. F. Chmelka and G. D. Stucky, *J. Am. Chem. Soc.*, 1998, **120**, 6024.
- 15 L. R. Melby, N. J. Rose, E. Abramson and J. C. Caris, *J. Am. Chem. Soc.*, 1964, **86**, 5117.
- 16 T. I. Morrow and E. J. Maginn, *J. Phys. Chem. B*, 2002, **106**, 12807.
- 17 Y. J. Li, B. Yan and Y. Li, *Microporous Mesoporous Mater.*, 2010, **131**, 82.
- 18 M. V. Landau, S. P. Varkey, M. Herskowitz, O. Regev, S. Pevzner, T. Sen and Z. Luz, *Microporous Mesoporous Mater.*, 1999, **33**, 149.

- 19 K. S. W. Sim, D. H. Everett, R. A. W. Haul, L. Moscow, R. A. Pierotti, J. Rouquerol and T. Siemieniowska, *Pure Appl. Chem.*, 1985, **57**, 603.
- 20 (a) Z. Y. Wu, Q. Jiang, Y. M. Wang, H. J. Wang, L. B. Sun, L. Y. Shi, J. H. Xu, Y. Wang, Y. Chun and J. H. Zhu, *Chem. Mater.*, 2006, **18**, 4600; (b) Z. H. Luan, M. Hartmann, D. Y. Zhao, W. Z. Zhou and L. Kevan, *Chem. Mater.*, 1999, **11**, 1621.
- 21 T. N. Martynova, L. D. Nikulina and V. A. Logvinenko, *J. Therm. Anal.*, 1990, **36**, 203.
- 22 (a) L. N. Sun, J. B. Yu, G. L. Zheng, H. J. Zhang, Q. G. Meng, C. Y. Peng, L. S. Fu, F. Y. Liu and Y. N. Yu, *Eur. J. Inorg. Chem.*, 2006, 3962; (b) A. A. S. Araujo, H. F. Brito, O. L. Malta, J. R. Matos, E. E. S. Teotonio, S. Storpirtis and C. M. S. Izumi, *J. Inorg. Biochem.*, 2002, **88**, 87.
- 23 (a) A. K. Singh, S. K. Singh, H. Mishra, R. Prakash and S. B. Rai, *J. Phys. Chem. B*, 2010, **114**, 13042; (b) V. Divya, S. Biju, R. Luxmi Varma and M. L. P. Reddy, *J. Mater. Chem.*, 2010, **20**, 5220;
- (c) Y. H. Zheng, Y. Li, C. L. Tan and Q. M. Wang, *Photochem. Photobiol.*, 2011, **87**, 641.
- 24 G. Vicentini, L. B. Zinner, J. Zukerman-Schpector and K. Zinner, *Coord. Chem. Rev.*, 2000, **196**, 353.
- 25 (a) M. H. V. Werts, R. T. F. Jukes and J. W. Verhoeven, *Phys. Chem. Chem. Phys.*, 2002, **4**, 1542; (b) C. Gorller-Walrand, L. Fluyt, A. Ceulemans and W. T. Carnall, *J. Chem. Phys.*, 1991, **95**, 3099.
- 26 P. Lenaerts, E. Ryckebosch, K. Driesen, R. Van Deun, P. Nockemann, C. Gorller-Walrand and K. Binnemans, *J. Lumin.*, 2005, **114**, 77.
- 27 L. R. Matthews and E. T. Knobbe, *Chem. Mater.*, 1993, **5**, 1697.
- 28 E. Huskowska, I. Turowska-Tyrk, J. Legendziewicz and J. P. Riehl, *New J. Chem.*, 2002, **26**, 1461.
- 29 E. E. S. Teotonio, J. G. P. Espinola, H. F. Brito, O. L. Malta, S. F. Oliveira, D. L. A. de Faria and C. M. S. Izumi, *Polyhedron*, 2002, **21**, 1837.
- 30 (a) Y. J. Li, B. Yan and Y. Li, *Chem.-Asian J.*, 2010, **5**, 1642; (b) Y. Y. Li, B. Yan, L. Guo and Y. J. Li, *Microporous Mesoporous Mater.*, 2012, **148**, 73.